Journal of Luminescence 170 (2016) 240–247

Contents lists available at ScienceDirect

Journal of Luminescence

journal homepage: www.elsevier.com/locate/jlumin

Full Length Article

Color tuning of Bi^{2+} luminescence in barium borates

Mathijs de Jong*, Andries Meijerink

Condensed Matter and Interfaces, Debye Institute for Nanomaterials Science, Utrecht University, Princetonplein 5, 3584 CC Utrecht, The Netherlands

ARTICLE INFO

Article history:
Received 4 August 2015
Received in revised form
15 October 2015
Accepted 16 October 2015
Available online 3 November 2015

Keywords:
Divalent bismuth
p–p transition
Barium borates
Narrow-band red phosphor
White light LEDs

ABSTRACT

The luminescence of Bi^{2+} has its origin in p–p transitions between different spin–orbit states in the $6s^26p^1$ electronic configuration. The divalent state is highly unusual for Bi and because of the low stability of Bi^{2+}, research on the intraconfigurational p–p transitions of Bi^{2+} is limited. Narrow-band emission has been observed in the orange/red spectral region, which makes Bi^{2+} luminescence interesting for application in white light LEDs. In this paper we investigate the luminescence of Bi^{2+} in a variety of borate host lattices with the aim to tune the emission wavelength and to investigate the influence of the host on the luminescence properties. Bi^{2+} was doped into $Sr_{1-x}Ba_xB_4O_7$, α-BaB_2O_4, α-BaB_4O_7, $Ba_2B_{10}O_{17}$ and BaB_8O_{13}. Luminescence was observed for Bi^{2+} in all hosts, except α-BaB_2O_4, indicating that Bi^{2+} cannot be stabilized in this host. In the other borates the emission wavelength varies between 586 nm (in BaB_8O_{13}) and 671 nm (in α-BaB_4O_7). The shift in emission wavelength is explained by a variation in crystal field splitting and spin–orbit coupling. The luminescence lifetime of the p–p emission is in the μs range, varying between 6 and 13 μs, reflecting the parity forbidden character of the p–p transition. Narrow-band red emission at 612 nm (FWHM=35 nm) is observed for $Ba_2B_{10}O_{17}$:Bi^{2+}. These luminescence characteristics of Bi^{2+} are favorable for application in w-LEDs, but an important drawback is that only low concentrations (in the ppm range) can be stabilized in the divalent state.

1. Introduction

The majority of luminescence studies on impurity doped inorganic compounds focuses on interconfigurational f–d transitions, on intraconfigurational d–d or f–f transitions and on charge transfer transitions. Intraconfigurational p–p transitions have hardly been studied, due to the lack of stable ions with a partially filled p-shell. The luminescence of the $6s^26p^1$ dopants Tl^0, Pb^+ and Bi^{2+} has been attributed to a p–p transition [1–4]. Due to spin–orbit coupling, there are two states within the $6s^26p^1$ electronic configuration: a $^2P_{1/2}$ ground state and a $^2P_{3/2}$ excited state. The excited state will split in two energy levels: $^2P_{3/2}(1)$ and $^2P_{3/2}(2)$, if the ion is situated at a site with low symmetry coordination (see Fig. 1). Because spin–orbit coupling increases strongly with atomic number, the p–p transitions in heavy elements are in the visible and near-infrared part of the spectrum.

Of the impurities Tl^0, Pb^+ and Bi^{2+}, the first two have only been observed in doped materials that have been irradiated with X-rays to create the unusual valence states by capturing free electrons generated by the ionizing radiation. Luminescence in thallium doped, X-ray irradiated alkali halides has been associated with p–p transitions on a combined Tl^0 – anion vacancy impurity [1]. In lead doped alkali halides that were X-ray irradiated, a variety of impurity centers with unusual oxidation states was found, including Pb^+ [3]. Of these three known $6s^26p^1$ dopants, only Bi^{2+} can be stabilized in a small number of hosts [4–11]. Blasse was in 1994 the first to ascribe the orange/red emission in Bi-doped SrB_4O_7 to the p–p transition $^2P_{3/2}(1) \rightarrow {}^2P_{1/2}$ in Bi^{2+} [4]. Recent *ab initio* energy level calculations have confirmed the hypothesis that this luminescence is due to the presence of Bi^{2+} on a Sr^{2+} site in SrB_4O_7, but the experiments also revealed that the concentration of Bi^{2+} is low, probably below ~20 ppm [12].

Borate and borophosphate host lattices of divalent cations like Ca^{2+}, Sr^{2+} and Ba^{2+} are known to stabilize the Bi^{2+} ion in low concentrations. A possible explanation for the suitability of these hosts is that they provide a rigid host lattice network with covalent character, which does not allow charge compensation mechanisms. This forces the bismuth to occupy a divalent cation site in the oxidation state of the host cation. There has not been a systematic study on the dependence of the luminescence properties of Bi^{2+} on the host lattice. Consequently, insight in variation of the emission color of the p–p transition by making use of the dependence of the spin–orbit coupling, crystal field splitting and the Stokes shift on the host lattice is limited.

In this paper we study the tunability of the Bi^{2+} emission by changing the host lattice in which bismuth is doped. First, we want to gain insight in the fundamental factors governing the absorption and emission properties of intraconfigurational p–p transitions,

* Corresponding author.
E-mail address: m.dejong3@uu.nl (M. de Jong).

http://dx.doi.org/10.1016/j.jlumin.2015.10.036
0022-2313/

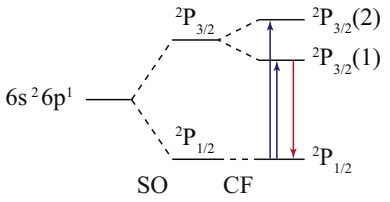

Fig. 1. Energy level diagram of the $6s^26p^1$ electronic configuration. Spin–orbit (SO) coupling splits the $6s^26p^1$ into a $^2P_{1/2}$ and $^2P_{3/2}$ term. In a low symmetry coordination the degeneracy of the $^2P_{3/2}$ state is lifted by the crystal field (CF) and this term splits in two levels: $^2P_{3/2}(1)$ and $^2P_{3/2}(2)$.

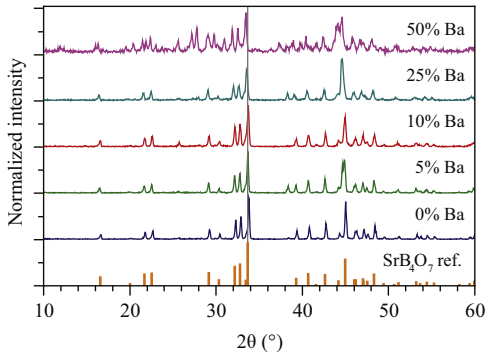

Fig. 2. X-ray powder diffractograms for $Sr_{1-x}Ba_xB_4O_7$ with $x=0$, 0.05, 0.1, 0.25 and 0.5. The PDF 04-008-1760 reference for SrB_4O_7 is shown at the bottom with the gray line indicating the position of the most intense line at 33.69° in the reference pattern.

since only limited information is available compared to the knowledge about intraconfigurational d–d and f–f transitions. Second, we are interested in tuning the emission of Bi^{2+} in such a way that it can be applied as activator in a narrow-band red emitting phosphor. Such a phosphor can be applied in white light LEDs, complementary to the YAG:Ce^{3+} phosphor that is now widely used to convert part of the blue light into yellow light. Presently most research on narrow-band red phosphors focuses on Eu^{2+} luminescence, which is characterized by emission with a FWHM of 50–70 nm. With a slight shift of the transition energies as observed for SrB_4O_7:Bi^{2+} (592 nm emission, FWHM=30 nm), Bi^{2+} emission might yield a suitable red phosphor with a maximum in the 610–620 nm range and a much narrower emission band than a typical Eu^{2+} emission band [7].

In the first part of this paper, we describe the possibility of tuning the luminescence properties of Bi^{2+} by partial substitution of Sr^{2+} with Ba^{2+} in SrB_4O_7:Bi^{2+}. In the second part, Bi^{2+} is incorporated in a variety of barium borates. The luminescence studies provide insight in the dependence of the transition energies on the host lattice and make it possible to test the hypothesis that a rigid host lattice is required for stabilizing Bi^{2+}.

2. Experimental details

Microcrystalline $Sr_{1-x}Ba_xB_4O_7$ (x=0, 0.05, 0.1, 0.25 and 0.50), α-BaB_2O_4, α-BaB_4O_7, $Ba_2B_{10}O_{17}$ and BaB_8O_{13} undoped and doped with 0.4 mol% bismuth (with respect to Sr/Ba in the starting mixture) were prepared by solid state synthesis. Stoichiometric amounts of $SrCO_3$, $BaCO_3$, H_3BO_3 and Bi_2O_3 were mixed and first fired for 2 h at 450 °C in a tube furnace under a N_2 flow, re-homogenized, and again fired in N_2 for 10 h at 840 °C for $Sr_{1-x}Ba_xB_4O_7$ and for 12 h at 825 °C for the barium borates. XRD characterization was performed with a Philips PW1820 diffractometer. Luminescence spectra were recorded using an Edinburgh FLS920 spectrofluorometer with a 450 W xenon lamp as excitation source and a Hamamatsu R928 PMT as detector. All excitation spectra were corrected for the intensity profile of the lamp and excitation monochromator and all emission spectra were corrected for the detection efficiency of the emission monochromator and PMT. Two-dimensional combined excitation/emission spectra were created by measuring a large number of emission spectra while stepwise varying the excitation wavelength. The decay times were measured using an Opotek Opolette 355 tunable laser in combination with the FLS920 spectrofluorometer, a Hamamatsu H7422-02 PMT and a EG&G Ortec Turbo-MCS.

3. Results and discussion

3.1. Co-doping of Ba^{2+} in SrB_4O_7:Bi^{2+}

To investigate the influence of partial replacement of Sr^{2+} by Ba^{2+} on the luminescence properties of Bi^{2+} in $Sr_{1-x}Ba_xB_4O_7$, a series of samples was prepared with $x=0$, 0.05, 0.1, 0.25 and 0.50. In Fig. 2 the X-ray diffractograms of the products are shown together with the reference diffractogram for SrB_4O_7. The diffractograms for the samples with up to 25% Ba^{2+} are very similar and show an XRD pattern that is consistent with the SrB_4O_7 crystal structure. Upon co-doping with barium, there is a small shift to smaller diffraction angles (see the gray line in Fig. 2, which indicates the reference position of the highest SrB_4O_7 diffraction peak) which is ascribed to a small increase in the lattice constant when the smaller Sr^{2+} ion is replaced by the larger Ba^{2+} ion. A continuous shift to smaller diffraction angles is commonly observed in solid solutions with the same crystal structure where a smaller ion is replaced by a larger ion and is known as Vegard's law [13].

For the sample with 50% Sr^{2+} and 50% Ba^{2+}, additional diffraction peaks are observed, indicating the presence of at least one other crystalline phase. This is not unexpected, since BaB_4O_7 has a different crystal structure than SrB_4O_7 and a stable solid solution cannot be formed over the full concentration range. For the present study, the luminescence properties of the samples with up to 25% Ba^{2+} are used to study the influence of barium co-doping on the Bi^{2+} transition energies.

In Fig. 3 the emission and excitation spectra of Bi^{2+}-doped $Sr_{1-x}Ba_xB_4O_7$ are shown. There is a single emission band in the orange/red spectral region, around 590–600 nm. The excitation spectrum shows two bands, one around 480 nm and one around 580 nm. Similar spectra have been reported before for Bi^{2+} in SrB_4O_7 [4,7]. The spectra in Fig. 3 look very similar and only small shifts are observed with the varying barium concentration. Both the excitation bands and the emission band shift to longer wavelengths upon increasing barium concentration. The maximum of the excitation peak for the $^2P_{1/2}\rightarrow{}^2P_{3/2}(2)$ transition shifts from 478.1 nm (0% Ba^{2+}) to 479.4 nm (25% Ba^{2+}), for the $^2P_{1/2}\rightarrow{}^2P_{3/2}(1)$ transition from 579.6 nm to 583.2 nm, while the emission corresponding to the $^2P_{3/2}(1)\rightarrow{}^2P_{1/2}$ transition shifts from 591.6 nm to 597.3 nm. This redshift is a combined effect of a varying Stokes shift, crystal field splitting and spin–orbit coupling as a function of Ba co-doping.

From the positions of the peaks, it is possible to calculate the Stokes shift, crystal field splitting and spin–orbit coupling for the Bi^{2+} ion. Upon increasing the barium concentration, the Stokes shift increases from 348 cm^{-1} (0% Ba^{2+}) to 405 cm^{-1} (25% Ba^{2+}). Considering the configuration coordinate diagram for electronic transitions, the magnitude of the Stokes shift is determined by the offset between the equilibrium positions in the two electronic states involved in the transition [14]. Because of the larger cation

site in the barium co-doped host compared to the barium-free host, there can be a larger relaxation in the excited state. This expansion leads to a larger offset, hence causing an increase of the Stokes shift upon barium co-doping.

The spin–orbit splitting between the $^2P_{1/2}$ and $^2P_{3/2}$ configurations of Bi^{2+} is determined by taking the energy difference between the ground state and the barycenter of the two excited state crystal field components, determined from the maxima of the two bands in the excitation spectra. The spin–orbit coupling decreases from 18910 cm^{-1} (0% Ba^{2+}) to 18802 cm^{-1} (25% Ba^{2+}) when barium is co-doped in SrB_4O_7:Bi^{2+}. The difference in spin–orbit coupling between the free ion (20,788 cm^{-1}, Ref. [15]) and the ion coordinated by ligands is a consequence of the nephelauxetic effect. This effect is caused by the delocalization of the electrons of the central ion over a larger volume as a result of covalent interactions between the central ion and its ligands. The decreased electron repulsion manifests as a decrease in energy of excited states. The last parameter that influences the excitation and emission energies is the magnitude of the crystal field splitting of the $^2P_{3/2}$ excited state, which we determined from the energy difference between the two band maxima in the excitation spectrum. Upon increasing the barium concentration, the splitting increases from 3665 cm^{-1} (0% Ba^{2+}) to 3714 cm^{-1} (25% Ba^{2+}).

Both the decreasing trend in spin–orbit splitting and the increasing trend in crystal field splitting upon co-doping with Ba^{2+} can be explained through the inductive effect. Ba^{2+} is more electropositive than Sr^{2+}, and therefore upon co-doping with Ba^{2+} more charge can be located on the oxygen ions. This has two consequences: (1) the covalency of the Bi^{2+}–O^{2-} bond increases, and therefore the spin–orbit splitting decreases, and (2) the increased charge on the coordinating oxygen increases the crystal field splitting for Bi^{2+} [22].

The changes in Stokes shift, spin–orbit coupling and crystal field splitting upon increasing the barium concentration are all small. To obtain full insight in the dependence of these parameters on the host lattice, *ab initio* calculations on this system are required. For example, the unexpected red-shift of Ce^{3+} d–f emission in YAG:Ce^{3+} upon co-doping with the large ion La^{3+} was explained by *ab initio* calculations as an effect of an anisotropic distortion around the Ce^{3+} ion. This distortion influences both the crystal field splitting and the centroid of the excited $5d^1$ states in Ce^{3+} [23,24].

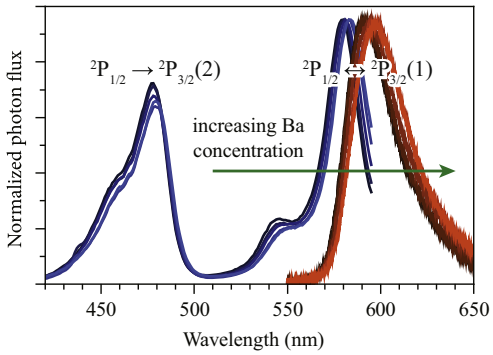

Fig. 3. Excitation (blue, $\lambda_{em} = 620$ nm) and emission (orange, $\lambda_{ex} = 480$ nm) spectra of $Sr_{1-x}Ba_xB_4O_7$ with $x=0$ (dark color), 0.05, 0.1, 0.25 and 0.5 (light color). Upon increasing barium co-doping concentration, the excitation and emission bands shift to longer wavelengths. (For interpretation of the references to color in this figure caption, the reader is referred to the web version of this paper.)

The normalized emission spectra for $Sr_{1-x}Ba_xB_4O_7$:Bi^{2+} with $x=0.25$ and 0.50 (Fig. 3) are almost equal, while the absolute emission intensity from the latter is weaker (not shown). The X-ray diffractograms showed that in the co-doped material with $x=0.50$, other phases (like BaO) are present in the material due to the limited solubility of Ba^{2+} in SrB_4O_7. In view of the limited stability of Bi^{2+}, it is not expected that Bi^{2+} is stable in these other phases. The observed luminescence for $Sr_{0.5}Ba_{0.5}B_4O_7$:Bi^{2+} originates therefore only from divalent bismuth in the $Sr_xBa_{1-x}B_4O_7$ phase. Because of the identical shape and position of the normalized emission spectra of $Sr_{0.75}Ba_{0.25}B_4O_7$:Bi^{2+} and $Sr_{0.5}Ba_{0.5}B_4O_7$:Bi^{2+}, it is concluded that the solubility limit of Ba^{2+} in SrB_4O_7 is around 25%. A further red shift of emission is therefore not possible by adding more Ba^{2+}.

3.2. Bi^{2+} doped in α-BaB_2O_4, α-BaB_4O_7, $Ba_2B_{10}O_{17}$ and BaB_8O_{13}

The shift in emission wavelength upon co-doping Bi^{2+}-doped SrB_4O_7 with barium shows that p–p transition energies can be tuned by varying the host lattice. Only a small shift can be induced for co-doping, as co-doping does not influence the structure of the host lattice. To study the influence of significant changes in the local surroundings, we synthesized four different bismuth-doped barium borates: α-BaB_2O_4, α-BaB_4O_7, $Ba_2B_{10}O_{17}$ and BaB_8O_{13}.

Almost all barium borates consist of BO_3 triangles and BO_4 tetrahedra forming a covalent framework in which the barium cations are embedded. The various barium borate structures are characterized by the BaO:B_2O_3 ratio of their molecular formula. Table 1 shows an overview of some of the structures that can be formed depending on the BaO:B_2O_3 ratio. The structures that were synthesized in this study are shown in bold.

It is seen in Table 1 that some of the host lattices have two different barium cation sites. This is expected to give rise to multiple peaks in the luminescence spectra of the bismuth doped borates as Bi^{2+} can substitute on two cation sites. The $^2P_{3/2}$ excited state of Bi^{2+} will split in two states, except in octahedral or tetrahedral symmetry. Since all the sites in Table 1 have a sufficiently low symmetry, the $^2P_{3/2}$ excited state of bismuth will split at all barium sites listed in the table.

Fig. 4 shows the X-ray diffractograms of the microcrystalline powders synthesized with the stoichiometric BaO:B_2O_3 ratios to form α-BaB_2O_4, α-BaB_4O_7, $Ba_2B_{10}O_{17}$ and BaB_8O_{13}. In this figure we overlapped the measured diffractograms (black) with the reference diffractogram of the expected structure (colored). In all four diffractograms the peaks corresponding to the expected crystal

Table 1
Overview of the barium borate structures that are discussed in this paper. The structural formulas in bold are the barium borates which were synthesized in this study. The references are ICDD PDF card numbers.

Compound	BaO:B_2O_3	Crystal system	Ba^{2+} sites and corresponding symmetries	XRD ref.
$Ba_2B_2O_5$	1:0.5	Monoclinic	unknown	00-024-0087
α–BaB_2O_4	1:1	Rhombohedral	1 × D_3 and 1 × C_3 (Ref. [16])	04-015-4055
α–BaB_4O_7	1:2	Monoclinic	2 × C_1 (1 × 9-coord, 1 × 10-coord) (Refs. [17,18])	04-011-6006
β-BaB_4O_7	1:2	Orthorhombic	1 × C_s (16-coord) (Ref. [19])	01-078-8545
$Ba_2B_{10}O_{17}$	1:2.5	Triclinic	2 × C_1 (1 × 10-coord, 1 × 11-coord) (Ref. [20])	00-028-0126
BaB_8O_{13}	1:4	Orthorhombic	1 × C_2 (Ref. [21])	00-020-0097

structure are present, thereby confirming a successful synthesis. However, for the α-BaB_2O_4, α-BaB_4O_7 and $Ba_2B_{10}O_{17}$ materials it is clear that additional peaks are observed in the diffractogram. These peaks are due to the presence of other barium borate phases in the material. In order to assign these peaks to their corresponding phases, the diffractograms are compared to references of other barium borate phases (colored, below the diffractogram). The peaks indicating the presence of these phases are marked with arrows (arrow color corresponding to reference color).

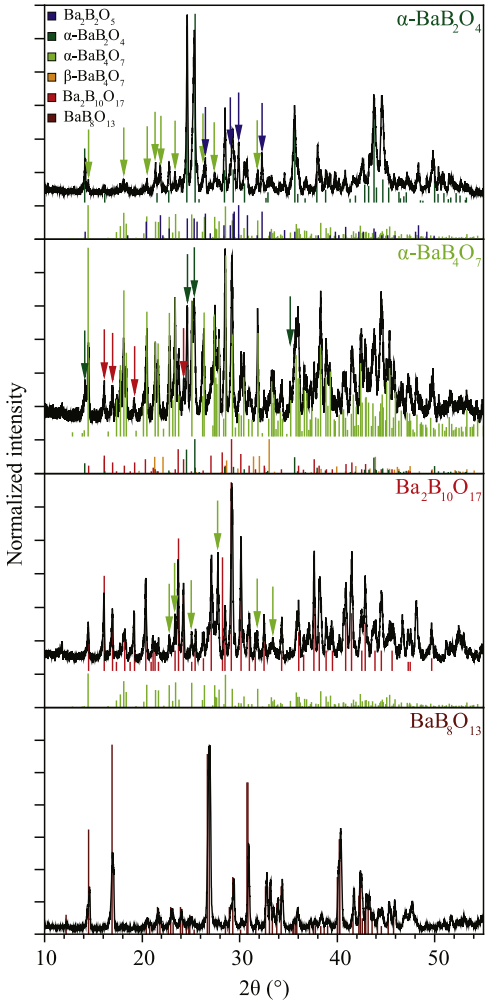

Fig. 4. X-ray powder diffractograms for materials with $BaO:B_2O_3$ ratios corresponding to α-BaB_2O_4 (1:1), α-BaB_4O_7 (1:2), $Ba_2B_{10}O_{17}$ (2:5) and BaB_8O_{13} (1:4). The black lines are the measured diffractograms, the overlapping colored lines correspond to reference diffractograms (see Table 1) of the expected structure. The diffractograms of α-BaB_2O_4, α-BaB_4O_7 and $Ba_2B_{10}O_{17}$ show additional peaks compared to the reference, which are attributed (colored arrows) to other barium borate phases (references in corresponding color below the diffractograms). (For interpretation of the references to color in this figure caption, the reader is referred to the web version of this paper.)

From the diffractograms in Fig. 4 it is concluded that the α-BaB_2O_4 material shows significant amounts of $Ba_2B_2O_5$ and α-BaB_4O_7 phase. Precise ratios cannot be given because the absolute diffraction intensities of the phases are not known, but we estimate that the order of magnitude for the fraction of both these impurity phases is around 10%. Also the α-BaB_4O_7 material shows phase impurity, with significant amounts of both α-BaB_2O_4 and $Ba_2B_{10}O_{17}$ phase present, probably on the order of 10–30%. No evidence was found for a β-BaB_4O_7 phase. The $Ba_2B_{10}O_{17}$ material contains only small quantities of α-BaB_4O_7, probably less than 10%. In the diffractogram of BaB_8O_{13} no traces of phase impurities are found.

The phase impurities in the barium borates are difficult to prevent. Since both phase impurities with a higher and lower BaO:B_2O_3 ratio are present in α-BaB_2O_4 and α-BaB_4O_7, changing the $BaO:B_2O_3$ ratio will not alleviate this problem. Also, longer reaction times did not improve the purity and higher reaction temperatures resulted in a glassy product. Obtaining phase pure borates is generally difficult and it is known to cause problems in phosphor synthesis [25].

The presence of multiple phases will influence the luminescence properties when these materials are doped with bismuth. Fig. 5 shows the combined excitation and emission spectra of the four bismuth-doped barium borates. To extract information on the luminescence of Bi^{2+} in each of the borates synthesized, emission spectra were recorded while changing the excitation wavelength in 3 nm steps. The resulting contour plots in Fig. 5 allow identification of excitation and emission bands for Bi^{2+} in the different borates, from the main crystalline phase as well as from impurity phases.

All bismuth doped barium borates in this study show only weak luminescence. The four bismuth-doped barium borates in Fig. 5 show multiple luminescence peaks, which correspond to excitation into the $^2P_{3/2}(2)$ level and emission from the $^2P_{3/2}(1)$ level. Excitation directly into the $^2P_{3/2}(1)$ level is also possible, but due to the very weak emission intensity, the presence of multiple excitation and emission bands and the small Stokes shift, it is experimentally difficult to record spectra for excitation in the $^2P_{3/2}(1)$ band. By combining the information from the phase impurities from Fig. 4 with the spectra in Fig. 5, it is possible to

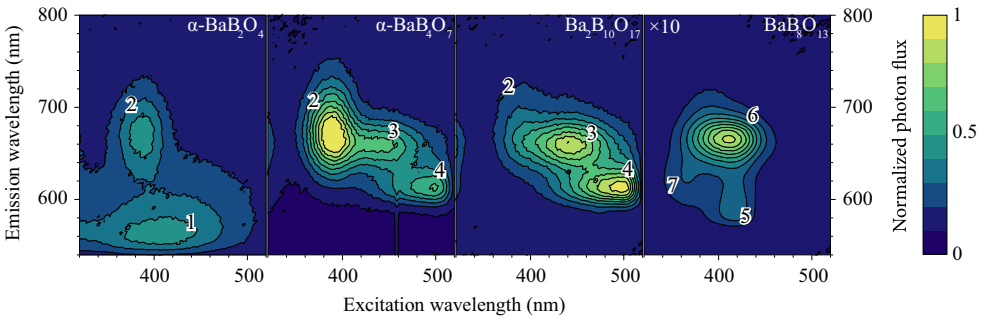

Fig. 5. Combined excitation and emission spectra for barium borates doped with bismuth. For all materials a spectrum of the undoped host lattice was also recorded. These background spectra, which were recorded under identical conditions, were subtracted from the spectra of the bismuth doped materials, to remove most of the background signal for these weakly luminescing materials. Note that the spectrum of BaB_8O_{13} is divided by ten, as Bi^{2+} in this host lattice showed a much stronger luminescence than in the other three materials. Bi^{2+} with excitation and emission bands at very similar spectral position are labelled 1–7, reflecting the seven Bi^{2+} centers that could be identified in the various borate hosts.

assign each luminescence peak to a specific barium borate phase. We will first assign all the peaks to their corresponding phases. After this we will describe the bismuth luminescence in each of the host lattices in more detail. To aid the discussion, we have labelled peaks with excitation and emission bands at the same wavelengths with numbers 1–7 (see Fig. 5).

Peak 1 in Fig. 5 only shows up in the spectrum of the α-BaB_2O_4 material. This material also contains significant amounts of $Ba_2B_2O_5$ and α-BaB_4O_7 phase. This peak is not observed in the α-BaB_4O_7 material, which also contains significant amounts of α-BaB_2O_4. For this reason peak 1 is attributed to the $Ba_2B_2O_5$ phase. The luminescence decay time of the emission of this peak is on the order of nanoseconds, which is much shorter than expected for Bi^{2+} luminescence and peak 1 is therefore assigned to luminescence from a defect, possibly created due to the presence of Bi^{3+}. As this peak does not give more information about Bi^{2+} luminescence, we will not discuss it further.

Peak 2 shows up in the spectrum of the α-BaB_2O_4 material and with higher intensity in the spectra of the α-BaB_4O_7 material. Luminescence decay times of 11.5 μs and 12.3 μs were measured for the 680 nm emission in the two hosts, indicating that these peaks in the two spectra belong to the same Bi^{2+} center. We assign this peak to luminescence of Bi^{2+} in the α-BaB_4O_7 phase. The low intensity of this peak in the α-BaB_2O_4 material is consistent with X-ray diffractograms, which show that there is a small amount of α-BaB_4O_7 phase present in the α-BaB_2O_4 material. In the same way, the very low intensity of this peak in the $Ba_2B_{10}O_{17}$ material is in agreement with the X-ray diffractograms of $Ba_2B_{10}O_{17}$, which showed that the concentration of α-BaB_4O_7 phase in the $Ba_2B_{10}O_{17}$ material is very low.

Peaks 3 and 4 are present in the spectrum of the α-BaB_4O_7 material, which has a significant amount of $Ba_2B_{10}O_{17}$ phase, and with higher intensity in the $Ba_2B_{10}O_{17}$ material. Based on the similar decay times of the peaks in the different materials (8.6 μs in α-BaB_4O_7 and 8.1 μs in $Ba_2B_{10}O_{17}$ for peak 3 and 5.8 μs in both materials for peak 4), we assign these peaks to luminescence of Bi^{2+} in the $Ba_2B_{10}O_{17}$ phase.

Finally, peaks 5, 6 and 7 are only observed in the BaB_8O_{13} material. As this material is phase pure, we assign all peaks to the BaB_8O_{13} phase. Peaks 5 and 6 show emission decay times of 13.0 μs and 13.1 μs and are therefore attributed to Bi^{2+} in this phase. The decay time of peak 7 could not be measured and this peak can therefore not with certainty be assigned to Bi^{2+}. In this host material there is only one cation site. Since peak 6 dominates in the spectrum of Bi-doped BaB_8O_{13}, we assign peak 6 to luminescence from Bi^{2+} on a Ba^{2+} lattice site.

The microsecond decay times and energies of the transitions are typical for the parity forbidden transitions within the 6p shell of the Bi^{2+} ion, as confirmed by *ab initio* calculations [12]. Because Bi^{3+} generally shows different luminescence properties (most commonly blue emission with nanosecond decay times at room temperature [26,27]), we assign peaks 2 to 6 all to Bi^{2+} in the various borate hosts.

A summary of the observed peaks is collected in Table 2. In this table we list the host lattice to which we assign the Bi^{2+} luminescence for each peak as well as the other materials in which we observed this peak due to phase impurities. The crystal field splitting Δ and the barycenter of the two excited states in this table are derived from the maxima of excitation and emission bands. The correct procedure is to use the zero-phonon lines, but these were not observed and their position is difficult to estimate due to the broad overlapping bands. Because of the difficulties in recording an excitation spectrum of the $^2P_{1/2} \rightarrow {}^2P_{3/2}(1)$ transition, the crystal field splitting is taken as the difference between maximum of the $^2P_{1/2} \rightarrow {}^2P_{3/2}(2)$ excitation band and the maximum of the $^2P_{3/2}(1) \rightarrow {}^2P_{1/2}$ emission band. By taking the maxima of the $^2P_{1/2} \rightarrow {}^2P_{3/2}(2)$ excitation and $^2P_{3/2}(1) \rightarrow {}^2P_{1/2}$ emission band instead of the zero-phonon lines, the crystal field splittings in Table 2 are systematically overestimated in the order of a thousand cm^{-1} and due to the possibility of a varying Stokes shift there is an uncertainty on the order of a few hundred cm^{-1}. We will now discuss in more detail the luminescence properties of Bi^{2+} in α-BaB_2O_4, α-BaB_4O_7, $Ba_2B_{10}O_{17}$ and BaB_8O_{13}.

3.2.1. α-BaB_2O_4

The structure of α-BaB_2O_4 consists of only BO_3 triangles [16], which form no extended covalently bound borate network. No rigid, covalent framework of BO_4 tetrahedra is present. We observed no Bi^{2+} emission in the α-BaB_2O_4 phase. This observation supports the hypothesis that a rigid, covalent framework which does not allow for charge compensation is essential to stabilize the divalent state of bismuth.

3.2.2. α-BaB_4O_7

The α-BaB_4O_7 structure consists of a three-dimensional framework of six-membered borate rings, linked together by multiple oxygen molecules. This extensively linked network of rings forms a rigid host for two different cation sites, 9- and 10-coordinated in the α-BaB_4O_7 phase [17].

Fig. 6 shows the excitation and emission spectra of α-BaB_4O_7:Bi^{2+}. The two characteristic bands that are observed in the excitation spectra of $Sr_{1-x}Ba_xB_4O_7$:Bi^{2+} are also seen in the excitation spectrum of α-BaB_4O_7:Bi^{2+}, corresponding to transitions from the $^2P_{1/2}$ ground state to the $^2P_{3/2}(1)$ and $^2P_{3/2}(2)$ energy levels. The emission spectrum in Fig. 6 shows one broad band at 671 nm

Table 2
Overview of Bi^{2+} luminescence peaks observed in the spectra of Fig. 5. We label the peaks according to the labels in Fig. 5 and tabulate the maximum of the $^2P_{1/2} \rightarrow {}^2P_{3/2}(2)$ excitation band (max λ_{ex}), the maximum of the $^2P_{3/2}(1) \rightarrow {}^2P_{1/2}$ emission band (max λ_{em}), crystal field splitting (Δ), the barycenter of the excited states $^2P_{3/2}(1)$ and $^2P_{3/2}(2)$, the phase to which the Bi^{2+} luminescence peak is assigned and other materials in which this luminescence peak (and phase) was observed.

No. in Fig. 5	max λ_{ex} (nm)	max λ_{em} (nm)	Δ[a] (10^3 cm^{-1})	Barycenter[b] (10^3 cm^{-1})	Assigned host lattice (decay time)	Also observed in material (decay time)
1	410	560			$Ba_2B_2O_5$	α-BaB_2O_4 (~ns, not Bi^{2+})
2	390	671	10.7	20.3	α-BaB_4O_7 (12.3 μs)	α-BaB_2O_4 (11.5 μs)
3	460	663	6.7	18.4	$Ba_2B_{10}O_{17}$ (8.1 μs)	α-BaB_4O_7 (8.6 μs)
4	503	612	3.5	18.1	$Ba_2B_{10}O_{17}$ (5.8 μs)	α-BaB_4O_7 (5.8 μs)
5	420	586	6.7	20.4	BaB_8O_{13} (13.0 μs)	
6	406	670	9.7	19.8	BaB_8O_{13} (13.1 μs)	
7	368	617	11.0	21.7	BaB_8O_{13} (not measured)	

[a] The crystal field splitting is taken as the difference between the maximum of the $^2P_{1/2} \rightarrow {}^2P_{3/2}(2)$ excitation band and the maximum of the $^2P_{3/2}(1) \rightarrow {}^2P_{1/2}$ emission band.

[b] The barycenter of the excited states is determined by taking the average of the excitation maximum of the $^2P_{3/2}(2)$ level and the emission maximum of the $^2P_{3/2}(1)$ level.

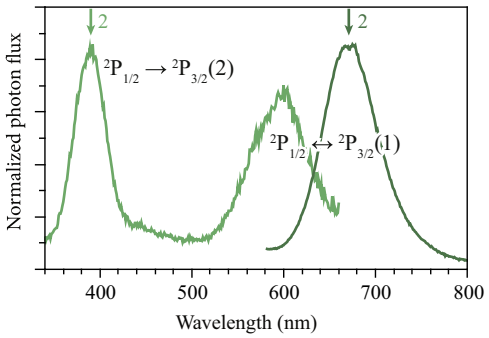

Fig. 6. The excitation (light green, $\lambda_{em} = 710$ nm) and emission (dark green, $\lambda_{ex} = 390$ nm) spectrum of Bi^{2+} in the α-BaB_4O_7 barium borate phase, corresponding to peak 2 in Fig. 5. (For interpretation of the references to color in this figure caption, the reader is referred to the web version of this paper.)

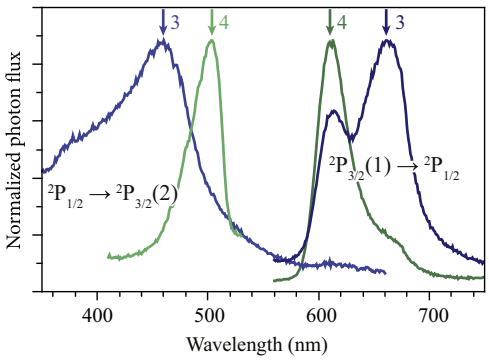

Fig. 7. The excitation (light color) and emission (dark color) spectra of Bi^{2+} in the $Ba_2B_{10}O_{17}$ barium borate phase, corresponding to peak 3 (blue color, $\lambda_{em} = 700$ nm and $\lambda_{ex} = 450$ nm) and peak 4 (green color, $\lambda_{em} = 610$ nm and $\lambda_{ex} = 505$ nm) in Fig. 5. (For interpretation of the references to color in this figure caption, the reader is referred to the web version of this paper.)

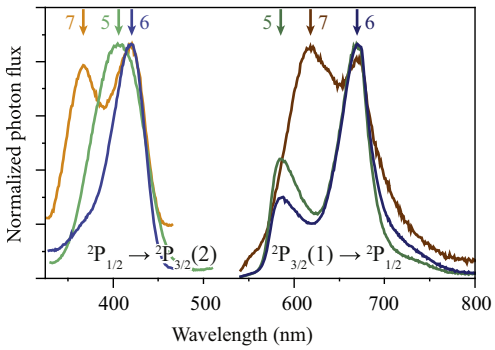

Fig. 8. The excitation (light color) and emission (dark color) spectra of Bi^{2+} in the BaB_8O_{13} barium borate phase, corresponding to peak 5 (green color, $\lambda_{em} = 685$ nm and $\lambda_{ex} = 425$ nm), peak 6 (blue color, $\lambda_{em} = 575$ nm and $\lambda_{ex} = 400$ nm) and peak 7 (orange/brown color, $\lambda_{em} = 620$ nm and $\lambda_{ex} = 360$ nm) in Fig. 5. (For interpretation of the references to color in this figure caption, the reader is referred to the web version of this paper.)

(FWHM = 70 nm), which is very broad compared to Bi^{2+} emission bands in other hosts.

In the emission spectrum of Fig. 6 a single emission band is observed, while there are two different cation sites in this lattice. In the 9-coordinated Ba^{2+} site the average distance between the central ion and the coordinating oxygen atoms is 2.81 Å, while in the 10-coordinated Ba^{2+} site this average distance is 2.94 Å [17]. In other hosts we found Bi^{2+} located on sites with ligand distances smaller than 2.81 Å and larger than 2.94 Å. For this reason it is likely that Bi^{2+} is located on both Ba^{2+} sites in α-BaB_4O_7. This observation, together with the very broad emission band, leads to the conclusions that the two emission bands originating from Bi^{2+} on the two crystallographic sites overlap in the peak at 671 nm.

3.2.3. $Ba_2B_{10}O_{17}$

The structure of $Ba_2B_{10}O_{17}$ consists of BO_3 triangles and BO_4 tetrahedra combined in a $B_{10}O_{23}$ building block, which forms a structure of infinite chains in which the cations are embedded. Two different cation sites are present, a 10-coordinated and an 11-coordinated site [20].

The spectra in Fig. 7 show the excitation and emission bands of Bi^{2+} in $Ba_2B_{10}O_{17}$. It was observed in Fig. 5 that two distinct emissions were present in the $Ba_2B_{10}O_{17}$ phase. The first emission peak at 612 nm (FHWM = 35 nm), the second peak has a maximum at 663 nm (FHWM ≈ 50 nm). The emission spectrum of the 663 nm emission (dark blue in Fig. 7) consists of the two peaks overlapping, as it is not possible to selectively excite only the emission at 663 nm without also exciting the emission at 612 nm.

So far we have seen that Bi^{2+} in different host lattices yields emission over the full orange/red range of the spectrum and the two luminescence peaks observed in bismuth-doped $Ba_2B_{10}O_{17}$ can be explained as luminescence of Bi^{2+} ions positioned at the two different cation sites that are present in $Ba_2B_{10}O_{17}$. In $Ba_2B_{10}O_{17}$ there is one 10-coordinated Ba^{2+} site with an average distance to the coordinating oxygen atoms of 2.86 Å and one 11-coordinated Ba^{2+} site with an average distance to the coordinating oxygen atoms of 2.95 Å. Due to the shorter distances of the ligands on the 10-coordinated site compared to the 11-coordinated site, we expect a bismuth ion substituted on the 10-coordinated site to experience a stronger crystal field splitting than on the 11-coordinated site. For this reason we assign peak 3 to the 10-coordinated site and peak 4 to the 11-coordinated site.

3.2.4. BaB_8O_{13}

The BaB_8O_{13} host lattice consists of two extended borate networks, both consisting of B_3O_5 and B_5O_8 groups. The available crystal structure data describe the presence of one distinct barium site [21].

The excitation and emission spectra of the three peaks that were observed in Fig. 5 are shown in Fig. 8. The emission intensity from Bi^{2+} in BaB_8O_{13} is an order of magnitude higher compared to Bi^{2+} in the other barium borate host lattices. This shows that the borate network of BaB_8O_{13} is suitable for the stabilization of relatively high concentrations of bismuth in its divalent oxidation state compared to the other barium borates host lattices. Nevertheless the luminescence intensity is still much weaker than in SrB_4O_7:Bi^{2+}.

The three luminescent species that are observed in Fig. 5 are not easy to separate as is evident from the spectra in Fig. 8. Peak 5 shows an excitation band with a maximum at 420 nm and an emission maximum at 586 nm (green line in Fig. 8). This emission cannot be excited selectively without also exciting the emission of

peak 6, which has an excitation maximum at 406 nm and an emission maximum at 670 nm (blue line in Fig. 8). The third emission band, peak 7, has an excitation maximum at 368 nm and an emission maximum at 617 nm (orange line in Fig. 8), which cannot be excited without also showing the emission of peak 6. The widths of the bands are difficult to determine, due to the strong overlapping of the bands, with the exception of peak 6 (FWHM = 40 nm).

The lifetime of peak 7 could not be measured in our lab since a pulsed excitation source of sufficiently short wavelength was not available, but the position and shape of its spectra suggest that this peak also belongs to luminescence from Bi^{2+}.

The occurrence of three distinct luminescence peaks is not in agreement with the reports that this host lattice has only one distinct Ba^{2+} site. However, Krogh-Moe reported that the details of the BaB_8O_{13} structure are "fairly inaccurate" due to the occurrence of crystal twinning [21]. Studies in which BaB_8O_{13} was doped with Ce^{3+} (Ref. [28]) and with Eu^{2+}/Eu^{3+} (Ref. [29]) have indicated that the dopants are present at at least two different Ba^{2+} sites. In the light of this information and the result from our experiment, it is necessary to obtain a more reliable crystal structure analysis of BaB_8O_{13} before we can assign the observed luminescence of Bi^{2+} in BaB_8O_{13} to specific crystallographic sites.

The luminescence properties of Bi^{2+} in the different barium borate host lattices are summarized in Table 2. It is clear from the luminescence in these different bismuth doped barium borate phases that the transition energies of Bi^{2+} depend on the crystalline environment of the ion. Emissions ranging from 586 nm (in BaB_8O_{13}) to 671 nm (in α-BaB_4O_7) were observed, covering the full orange/red part of the spectrum. The shift in emission wavelength is caused both by a variation in crystal field splitting and nephelauxetic effect. The crystal field splitting on Bi^{2+} shows a large variety, from $3.5 \cdot 10^3$ cm^{-1} for one specific site in $Ba_2B_{10}O_{17}$ to the unexpectedly large crystal-field splitting of $11.0 \cdot 10^3$ cm^{-1} for one specific site in BaB_8O_{13}. The spin–orbit coupling, which varies due to the earlier described nephelauxetic effect, shows a smaller variation, between $18 \cdot 10^3$ cm^{-1} and $22 \cdot 10^3$ cm^{-1}, which is in line with the expectation that the local coordination mostly influences the crystal field splitting.

Recent *ab initio* calculations have shown that the symmetry of the local crystal field around Bi^{2+} has a large influence on the crystal field splitting between the $^2P_{3/2}(1)$ and $^2P_{3/2}(2)$ levels [30]. It was shown that especially tetragonal and orthorhombic distortions from a perfect cubic coordination lead to a large crystal field splitting. The large spread in crystal field splitting in our experiments confirms the large influence of the host lattice. Because of the relatively small variation in distance to the ligands from 2.81 Å to 2.95 Å in the various lattices, we do not expect a variation of the crystal field splittings over a factor three. The strong influence of the symmetry of the coordinating ligands, as described by Seijo [30], can therefore be an explanation of our observations.

Due to the small number of studies that have been performed on the Bi^{2+} ion, no ionic radius of this ion is known. Because of the relatively successful incorporation of Bi^{2+} on a Sr^{2+} site in SrB_4O_7 (Sr^{2+} 9-coordinated, ionic radius 1.45 Å, Ref. [31]) and because of the low intensity of Bi^{2+} luminescence in all the barium borates (Ba^{2+} 9-coordinated, ionic radius 1.61 Å, Ref. [31]), we expect the ionic radius of Bi^{2+} on a 9-coordinated site to be close to 1.45 Å.

The 612 nm emission in $Ba_2B_{10}O_{17}$:Bi^{2+} has potential as a narrow-band red emitter in a white light LED. The center of this emission peak is at a suitable wavelength for a good color rendering index (CRI) and the width of the band (35 nm) is small compared to red Eu^{2+} phosphors (FWHM typically 50–70 nm) that are commonly used in solid state lighting nowadays [32]. However, of the two cation sites in $Ba_2B_{10}O_{17}$, only the one responsible for the 612 nm emission is favorable for w-LEDs and it will be difficult to dope bismuth selectively on one specific site. Another important step in making Bi^{2+} luminescence applicable in solid state lighting is to investigate ways to increase the concentration of Bi^{2+} stable in borate host lattices, as the luminescence from bismuth in the barium borates discussed here is very weak due to extremely low (ppm) doping levels.

4. Conclusions

In this study we have investigated the influence of the local coordination on the luminescence of divalent Bi^{2+}, an unusual oxidation state for Bi. Intraconfigurational p–p transitions between the $^2P_{3/2}$ excited state and $^2P_{1/2}$ ground state give rise to narrow band emission in the orange-red spectral region. To investigate the influence of the host lattice on the luminescence properties, Bi^{2+} has been incorporated in a variety of borate host lattices.

In SrB_4O_7 tuning of the Bi^{2+} is possible in solid solutions of (Sr, Ba)B_4O_7. Up to 25% of Sr^{2+} can be replaced by Ba^{2+} and induces a small red shift of the Bi^{2+} emission (from 591.6 to 597.3 nm). A wider tuning range is achieved by incorporating Bi^{2+} in different borate host lattices. Bi^{2+} was successfully doped into α-BaB_4O_7, $Ba_2B_{10}O_{17}$ and BaB_8O_{13}, all host lattices with a rigid borate network. For α-BaB_2O_4 no Bi^{2+} emission was observed, indicating that Bi^{2+} cannot be stabilized in this host. This is explained by the absence of a borate network in the α-BaB_2O_4 structure. A rigid network with a covalent framework seems to be required as otherwise charge compensation allows oxidation of Bi to higher, more stable valence states. For Bi^{2+} in the three borate hosts emission bands were observed for Bi^{2+} on different crystallographic sites with emission maxima ranging from 586 nm (in BaB_8O_{13}) to 671 nm (in α-BaB_4O_7). The emission bands are narrow (typical FWHM of 30–40 nm) and the decay time for the parity forbidden p–p transitions is around 10 μs. A lower coordination number and smaller Bi^{2+}–O^{2-} distances shift the emission to longer wavelengths because of a larger crystal field splitting of the $^2P_{3/2}$ excited state, pushing the emitting $^2P_{3/2}(1)$ state towards lower energies. The coordination also affects the emission wavelength through the nephelauxetic effect and Stokes shift.

The ability to tune the narrow band Bi^{2+} emission in the orange-red spectral region makes Bi^{2+} promising for application in luminescent materials, e.g. as a narrow band red emitter in energy efficient warm white LEDs. The limited stability of Bi^{2+} however hampers application as only very low doping concentrations (ppm level) of Bi^{2+} can be achieved, preventing strong absorption required for most applications.

Acknowledgements

This work is financed by the EU Marie Curie Initial Training Network LUMINET (316906). We want to acknowledge Michiel Bruins and Stefan Gaillard for their contributions on bismuth doped $Sr_{1-x}Ba_xB_4O_7$.

References

[1] M. Fockele, F.J. Ahlers, F. Lohse, J.-M. Spaeth, R.H. Bartram, J. Phys. C: Solid State Phys. 18 (1985) 1963.
[2] L.F. Mollenauer, N.D. Vieira, L. Szeto, Phys. Rev. B 27 (1983) 5332.
[3] M. Fockele, F. Lohse, J.-M. Spaeth, R.H. Bartram, J. Phys.: Condens. Matter 1 (1989) 13.
[4] G. Blasse, A. Meijerink, M. Nomes, J. Zuidema, J. Phys. Chem. Solids 55 (1994) 171.
[5] A.M. Srivastava, J. Lumin. 78 (1998) 239.
[6] Q. Zeng, T. Zhang, Z. Pei, Q. Su, J. Mater. Sci. Technol. 15 (1999) 281.
[7] M. Peng, L. Wondraczek, Opt. Lett. 34 (2009) 2885.
[8] M. Peng, L. Wondraczek, J. Am. Ceram. Soc. 93 (2010) 1437.

[9] M. Peng, L. Wondraczek, Opt. Lett. 35 (2010) 2544.
[10] M. Peng, J. Lei, L. Li, L. Wondraczek, Q. Zhang, J. Qiu, J. Mater. Chem. C 1 (2013) 5303.
[11] R. Cao, F. Zhang, C. Liao, J. Qiu, Opt. Express 21 (2013) 15728.
[12] M. de Jong, A. Meijerink, R.A. Gordon, Z. Barandiarán, L. Seijo, J. Phys. Chem. C 118 (2014) 9696.
[13] L. Vegard, Z. Phys. 5 (1921) 17.
[14] M. de Jong, L. Seijo, A. Meijerink, F.T. Rabouw, Phys. Chem. Chem. Phys. 17 (2015) 16959.
[15] A. Kramida, Yu. Ralchenko, J. Reader, NIST ASD Team, NIST Atomic Spectra Database (ver. 5.1), National Institute of Standards and Technology, Gaithersburg, MD, 2013, Available Online at: http://physics.nist.gov/asd [2015, June 18].
[16] A.D. Mighell, A. Perloff, S. Block, Acta Cryst. 20 (1966) 819.
[17] S. Block, A. Perloff, Acta Cryst. 19 (1965) 297.
[18] W.-D. Stein, J. Liebertz, P. Becker, L. Bohatý, M. Braden, Eur. Phys. J. B 85 (2012) 236.
[19] J.S. Knyrim, S.R. Römer, W. Schnick, H. Huppertz, Solid State Sci. 11 (2009) 336.
[20] L. Liu, X. Su, Y. Yang, S. Pan, X. Dong, S. Han, M. Zhang, J. Kang, Z. Yang, Dalton Trans. 43 (2014) 8905.
[21] J. Krogh-Moe, M. Ihara, Acta Cryst. B 25 (1969) 2153.
[22] A.M. Srivastava, Opt. Mater. 31 (6) (2009) 881.
[23] K. Li, G. Shucai, H. Guangyan, Z. Jilin, J. Rare Earth 25 (2007) 692.
[24] A.B. Mu noz García, J.L. Pascual, Z. Barandiarán, L. Seijo, Phys. Rev. B 82 (2010) 064114.
[25] L.J.Q. Maia, C.R. Ferrari, V.R. Mastelaro, A.C. Hernandes, A. Ibanez, Solid State Sci. 10 (2008) 1835.
[26] A. Wolfert, G. Blasse, J. Solid State Chem. 59 (1985) 133.
[27] A. Wolfert, E.W.J.L. Oomen, G. Blasse, J. Solid State Chem. 59 (1985) 280.
[28] T. Koskentalo, M. Leskela, J. Less-Common Met. 112 (1985) 67.
[29] L. He, Y. Wang, W. Sun, J. Rare Earth. 27 (2009) 385.
[30] L. Seijo, Z. Barandiarán, Phys. Chem. Chem. Phys. 16 (2014) 17305.
[31] R.D. Shannon, Acta Crystallogr. A 32 (1976) 751.
[32] P.F. Smet, A.B. Parmentier, D. Poelman, J. Electrochem. Soc. 158 (2011) R37.